

Elliptic Flow and the Nuclear Equation of State

W. TRAUTMANN and H. H. WOLTER

*GSI Helmholtzzentrum für Schwerionenforschung GmbH
Planckstr. 1, D-64291 Darmstadt, Germany
w.trautmann@gsi.de*

*Fakultät für Physik, Universität München
Am Coulombwall 1, D-85748 Garching, Germany
hermann.wolter@lmu.de*

New constraints for the nuclear equation of state at suprasaturation densities have been obtained by measuring collective particle flows in heavy-ion reactions at relativistic energies. Ratios and differences of neutron and hydrogen flows in $^{197}\text{Au} + ^{197}\text{Au}$ collisions at 400 MeV/nucleon were used in studies of the asymmetric-matter equation of state. The comparison with predictions of transport models favors a moderately soft to linear density dependence, consistent with ab-initio nuclear matter theories. Model predictions suggest that comprehensive data sets collected at higher bombarding energies will provide information on the asymmetric-matter equation of state in the density range up to two or three times the saturation value.

1. Introduction

Collective nuclear motion has always been a topic followed and advanced by Walter Greiner. His seminal papers on nuclear collective excitation from the 60s of last century have guided a generation of nuclear structure physicists.^{1,2} The investigation and description of density oscillations of small amplitude have not only enhanced our knowledge about the collective degrees of freedom of atomic nuclei but have also revealed fundamental properties of nuclear matter. The nuclear compressibility is of importance for many phenomena in nuclear structure and nuclear reactions as well as for astrophysics.

To go beyond the small density interval probed with giant resonances requires nuclear reactions. In their famous shock-wave paper of 1974, Scheid, Müller and Greiner have studied new phenomena produced by the collective pressure in the shock-compressed overlap zone.³ They have shown that heavy-ion reactions at sufficiently high energy provide us with the possibility to compress nuclear matter

up to several times the saturation density ρ_0 encountered in the interior of heavy nuclei. The properties of nuclear matter at suprasaturation densities may thus be studied in laboratory experiments.⁴ From the extensive search for observables suitable for probing the brief high-density phase of the collision, collective flows and sub-threshold production of strange mesons have appeared as most useful. A consensus has been reached that a soft equation of state (EoS), corresponding to a compressibility $K \approx 200$ MeV and including momentum dependent interactions, best describes the high-density behavior of symmetric nuclear matter. It is based on studies of flow and kaon production within the framework of transport theory.⁴⁻⁶ This finding has very recently been confirmed in a new analysis of the high-precision flow data measured by the FOPI Collaboration at the GSI laboratory.^{7,8} We may note here that the conclusion that K should be of the order of 200 MeV was presented by Greiner and coworkers 49 years ago, based on a theoretical analysis of the elastic-scattering excitation function for $^{16}\text{O} + ^{16}\text{O}$ measured by the Yale group.⁹

In recent years, motivated by the impressive progress made in observing properties of neutron stars and in understanding details of supernova explosion scenarios, the EoS of neutron-rich asymmetric matter has received increasing attention.¹⁰⁻¹³ The symmetry energy, equal to the difference between the energies per nucleon of neutron matter and of symmetric matter, is seen as one of the biggest unknowns in this context. We have precise information on the symmetry energy near saturation density from the knowledge of nuclear masses. For densities below saturation, investigations of nuclear structure phenomena and of heavy ion reactions in the Fermi energy regime have constrained the symmetry energy considerably.¹⁴⁻¹⁶ The importance of clustering at subsaturation densities has recently been demonstrated¹⁷ and confirmed in comparison with experimental data from intermediate-energy reactions.¹⁸⁻²⁰ At suprasaturation density, however, the symmetry energy is still largely unknown for several reasons. Phenomenological forces, even though well constrained near saturation, yield largely diverging results if they are extrapolated to higher densities.^{21,22} Many-body calculations with realistic potentials face the problem that three-body forces and short-range correlations are not sufficiently constrained at the higher densities at which their importance increases.²³⁻²⁶ Even the magnitude of the kinetic contribution is possibly modified by a redistribution of nucleon momenta due to short-range correlations in high-density nuclear matter.²⁷⁻²⁹

The symmetry energy appears in nearly every aspect of nuclear structure and reactions and, as a consequence, a variety of constraints obtained with different methods have become available.³⁰ However, quantities as, e.g., the thickness of the neutron skin in heavy nuclei or the isospin transport in reactions of isospin-asymmetric nuclei in the Fermi-energy domain are predominantly sensitive to the strength of the symmetry term at densities near or below the saturation value.^{11,14,15,31-34} The example shown by Brown³⁵ demonstrates that a very precise knowledge of the neutron-skin thickness of ^{208}Pb will be required if an extrapolation from density $\rho \approx 0.6\rho_0$, where the symmetry energy is well determined, to the saturation density

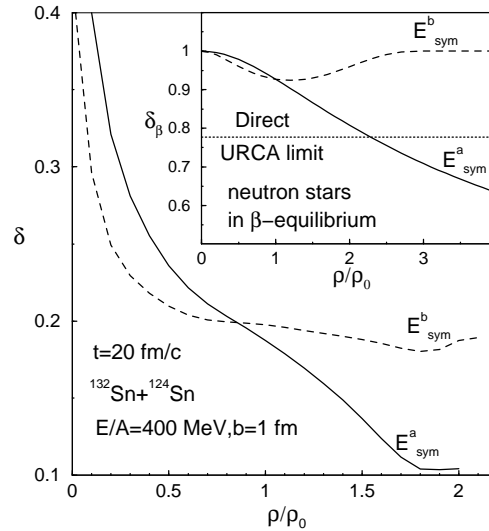


Fig. 1. Isospin asymmetry $\delta = (\rho_n - \rho_p)/\rho$ as a function of the normalized density ρ/ρ_0 at time $t = 20$ fm/c in the $^{132}\text{Sn} + ^{124}\text{Sn}$ reaction with a stiff (E_{sym}^a) and with a soft (E_{sym}^b) density dependence of the nuclear symmetry energy. The corresponding correlation for neutron stars in β -equilibrium is shown in the inset (reprinted with permission from Ref. 36; Copyright (2002) by the American Physical Society).

ρ_0 is attempted. This emphasizes the need for more direct high-density probes. As in the case of symmetric nuclear matter, collective flows and sub-threshold particle production are obvious candidates.

A strong motivation for exploring the information contained in isotopic flows was provided some time ago by Bao-An Li when he pointed to the parallels in the density-dependent isotopic compositions of neutron stars and of the transient systems formed in collisions of neutron-rich nuclei depending on the EoS input used in the calculations.³⁶ Figure 1 illustrates the remarkable fact that the same physical laws govern objects differing by 18 orders of magnitude in linear scale or 55 orders of magnitude in mass. Properties of exotic astrophysical objects may thus be inferred from data obtained in laboratory experiments, and vice versa. A main difficulty resides in the comparatively small asymmetry of atomic nuclei available for experiments. Symmetry effects are, therefore, always small relative to those of the dominating isoscalar forces. A partial cancellation of the latter may be expected in differences or ratios of observables between isotopic partners.

A further encouragement was provided by transport model calculations indicating that the elliptic flows of free neutrons and free protons respond differently to variations of the parametrization of the symmetry energy.³⁷ Elliptic flow refers to the second Fourier component of the azimuthal anisotropy of particle emissions. It has motivated a reanalysis of the FOPI-LAND data for $^{197}\text{Au} + ^{197}\text{Au}$ collisions at 400 MeV/nucleon, collected many years ago and used to demonstrate the existence of neutron squeeze-out in this energy regime.^{38,39} Squeeze-out refers to a dominant

out-of-plane emission of particles, relative to in-plane emission, and is considered as evidence for the pressure buildup in the collision zone. It should therefore be particularly sensitive to the high-density EoS. The analysis has favored a moderately soft to linear density dependence of the symmetry energy.^{37,40}

This finding had a particular significance, in spite of a large statistical uncertainty. Rather different conclusions, ranging from a super-soft to a super-stiff behavior of the symmetry energy, had previously been reached in analyses of the π^-/π^+ production ratios, measured by the FOPI Collaboration⁴¹ for the same $^{197}\text{Au} + ^{197}\text{Au}$ reaction, with different transport models.^{42–45} In particular, the super-soft result, first presented by Xiao *et al.*,⁴³ has initiated a broad discussion of how it might be reconciled with other observations as, e.g., properties of neutron stars.^{43,46,47} The FOPI-LAND elliptic-flow data were found to be inconsistent with this extreme assumption and, in fact, fairly independent of particular choices made for the model parameters used for the quantum-molecular-dynamics (QMD) transport-model calculations.^{37,48}

The obvious need to improve the statistical accuracy beyond that of the existing data set has initiated a dedicated measurement by the ASY-EOS Collaboration of collective flows in collisions of $^{197}\text{Au} + ^{197}\text{Au}$ as well as of $^{96}\text{Zr} + ^{96}\text{Zr}$ and $^{96}\text{Ru} + ^{96}\text{Ru}$. It was carried out in 2011 at the GSI laboratory with the LAND⁴⁹ detector coupled to a subset of the CHIMERA⁵⁰ detector array.⁵¹ In the following sections, the present situation will be described in relation to the new results from the ASY-EOS experiment.

2. Present Knowledge of the Symmetry Energy

Our knowledge of the symmetry energy is originally based on nuclear masses whose dependence on the isotopic composition is reflected by the symmetry term in the Bethe-Weizsäcker mass formula. A density dependence is already indicated by the use of separate bulk and surface terms in refined mass formulae. In the Fermi-gas model, it is given by a proportionality to $(\rho/\rho_0)^\gamma$ with an exponent $\gamma = 2/3$, where $\rho_0 \approx 0.16$ nucleons/fm³ is the saturation density. This kinetic contribution to the symmetry energy, however, amounts to only about 1/3 of the symmetry term of approximately 30 MeV for nuclear matter at saturation. The major contribution is given by the potential term reflecting properties of the nuclear forces.

Nuclear many-body theory has presented us with a variety of predictions for the nuclear equation of state.^{4,11,22,52–54} The examples shown in Fig. 2 for the two cases of symmetric nuclear matter and of pure neutron matter demonstrate that, overall, the results are quite compatible among each other, except for densities exceeding saturation at which the predictions diverge. The symmetry energy E_{sym} can be defined as the coefficient of the quadratic term in an expansion of the energy per particle in the asymmetry $\delta = (\rho_n - \rho_p)/\rho$, where ρ_n, ρ_p , and ρ represent the neutron, proton, and total densities, respectively,

$$E/A(\rho, \delta) = E/A(\rho, \delta = 0) + E_{\text{sym}}(\rho) \cdot \delta^2 + \mathcal{O}(\delta^4). \quad (1)$$

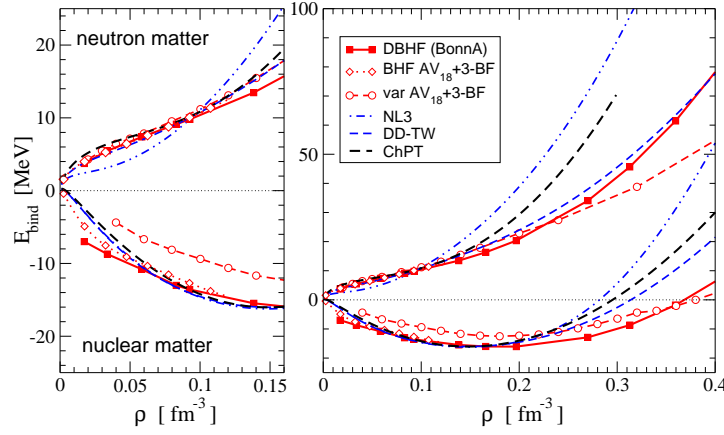


Fig. 2. EoS in nuclear matter and neutron matter as a function of density. BHF/DBHF and variational calculations with realistic forces are compared to phenomenological density functionals NL3 and DD-TW and to ChPT. The left panel zooms the low density range (from Ref. 22, reprinted with kind permission from Springer Science+Business Media).

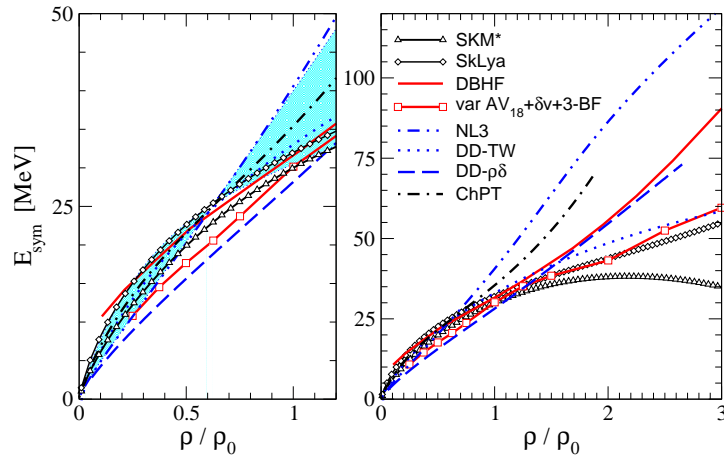


Fig. 3. Symmetry energy as a function of density as predicted by different models. The left panel zooms the low density range up to saturation. The full lines represent the DBHF and variational approaches using realistic forces (from Ref. 22, reprinted with kind permission from Springer Science+Business Media).

In the quadratic approximation, the symmetry energy is the difference between the energies of symmetric matter ($\delta = 0$) and neutron matter ($\delta = 1$). It is shown in Fig. 3 for a similar range of models as in Fig. 2. Also the symmetry energy diverges at high density, as expected from Fig. 2, while most empirical models coincide near or slightly below saturation, the density range at which constraints from finite nuclei are valid.

In calculations using realistic forces fitted to two- and three-nucleon data, the

uncertainty is mainly related to the short-range behavior of the nucleon-nucleon force and, in particular, to the three-body and tensor forces.^{23–26} The three-body force has been shown to make an essential but quantitatively small contribution to the masses of light nuclei.⁵⁵ The extrapolation of the partly phenomenological terms used there to higher densities is, however, highly uncertain.²⁵ The general effect of including three-body forces in the calculations is a stiffening of the symmetry energy with increasing density.^{56,57} Short-range correlations become also increasingly important at higher densities. Results from very recent new experiments will, therefore, have a strong impact on predictions for high-density nuclear matter.^{23,24,27–29} Data from neutron-star observations provide important constraints already now.⁵⁸ With the improvement of observational methods, they will become more stringent in the near future.⁵⁹

At higher energies, the momentum dependence of the nuclear forces becomes important.^{11,12,60,61} It is well known that nuclear mean fields are momentum dependent, as seen, e.g., in the energy dependence of the nuclear optical potential. The dominating effect is in the isoscalar sector but there is also an important isovector momentum dependence. It manifests itself as an energy dependence of the isospin-dependent part of the optical potential but can also be expressed in terms of a difference of the effective masses of protons and neutrons.²² Even the ordering of these effective masses is still an open problem.^{30,62,63} It has, moreover, been shown that the effective mass differences and the asymmetry dependence of the EoS are both influencing particle yields and flow observables, and that additional observables will be needed to resolve the resulting ambiguity.^{12,60,61,64}

Transport theories needed for calculating the temporal evolution of nuclear reactions often use simplified descriptions of the composition-dependent part of the nuclear mean field. In the UrQMD of the group of Li and Bleicher,⁶⁵ the potential part of the symmetry energy is defined with two parameters, the value at saturation density, usually taken as 22 MeV in their calculations, and the power-law coefficient γ describing the dependence on density,

$$E_{\text{sym}} = E_{\text{sym}}^{\text{pot}} + E_{\text{sym}}^{\text{kin}} = 22 \text{ MeV} \cdot (\rho/\rho_0)^\gamma + 12 \text{ MeV} \cdot (\rho/\rho_0)^{2/3}. \quad (2)$$

In other codes the nuclear potential of Das *et al.* with explicit momentum dependence in the isovector sector is used.⁶⁶ There, as in the Boltzmann-Uehling-Uhlenbeck-type code IBUU04 developed by the groups of Li and Chen,^{11,67} the density dependence of the symmetry energy is characterized by a parameter x appearing in the potential expressions. Examples of these parametrizations and of results obtained from the analysis of experimental reaction data are given in Fig. 4. The stiff (E_{sym}^a) and soft (E_{sym}^b) density dependences of Fig. 1 correspond approximately to the cases $\gamma = 1$ and $x = 1$ shown here. Density functionals of the Skyrme type are also increasingly used in transport model calculations.^{63,68}

Parametrizations of this kind have the consequence that, once the symmetry energy at the saturation point is fixed, a single value at a different density or, alternatively, the slope or curvature at any density will completely determine the

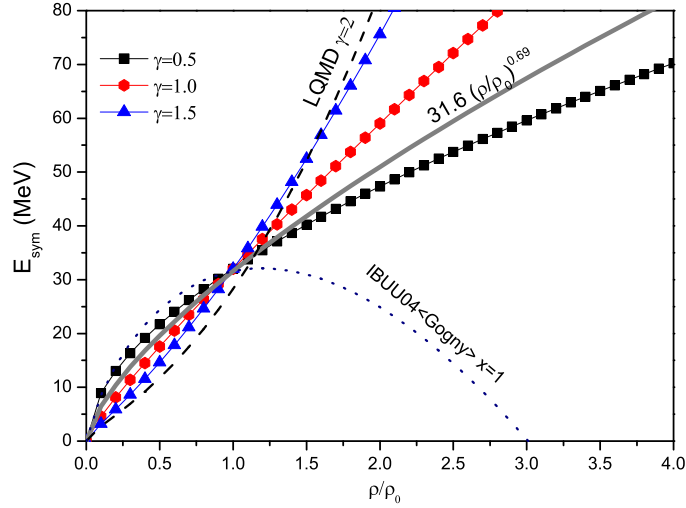


Fig. 4. Parametrizations of the nuclear symmetry energy as used in transport codes: three parametrizations of the potential term used in the UrQMD (Ref. 65) with power law coefficients $\gamma = 0.5, 1.0$, and 1.5 (lines with symbols as indicated), the result with $\gamma = 0.69$ obtained from analyzing isospin diffusion data with the IBUU04 (full line, Ref. 67), and the super-soft and stiff parametrizations obtained from analyzing the π^-/π^+ production ratios with the IBUU04 (dotted line, Ref. 43) and the LQMD (dashed line, Ref. 44) transport models (from Ref. 69, reprinted with kind permission from Springer Science+Business Media).

parametrization. Measurements of a variety of observables in nuclear structure and reactions have, in this manner, been used to obtain results for the density dependence of the symmetry energy. They are conventionally expressed in the form of the parameter L which is proportional to the slope at saturation,

$$L = 3\rho_0 \cdot dE_{\text{sym}}/d\rho|_{\rho_0}. \quad (3)$$

Most results with their errors fall into the interval $20 \text{ MeV} \leq L \leq 100 \text{ MeV}$ and are compatible with a most probable value $L \approx 60 \text{ MeV}$, roughly corresponding to a power-law coefficient $\gamma = 0.6$.^{11,14,15,30,46,70} The full line in Fig. 4 represents, e.g., the result deduced by Li and Chen from the MSU isospin-diffusion data and the neutron-skin thickness in ^{208}Pb .⁶⁷ The corresponding slope parameter is $L = 65 \text{ MeV}$. Rather similar constraints have been deduced from recent investigations and observations of neutron-star properties.^{26,57,58}

Considerable progress regarding the correlation of the symmetry energy with particular observables in different models has been made by the Florida and Barcelona groups.^{71,72} In continuation of the work of Typel and Brown⁷³ and of Furnstahl,⁷⁴ a universal correlation between the thickness of the neutron-skin of ^{208}Pb and the L parameter has been found for empirical mean-field interactions.⁷² The determination of the neutron-skin thickness by measuring the parity-violating contribution to electron scattering at high energy will thus offer a practically model-free access to the slope at saturation.^{75,76}

3. Probing High Densities

Densities of two to three times the saturation density may be reached on time scales of $\approx 10\text{--}20\text{ fm}/c$ in the central zone of heavy-ion collisions at relativistic energies of up to $\approx 1\text{ GeV/nucleon}$.^{77,78} The resulting pressure produces a collective outward motion of the compressed material whose strength will be influenced by the symmetry energy in asymmetric systems.^{4,79} At the same time, the excitation of Δ resonances in hard nucleon-nucleon scatterings leads to the production and subsequent emission of charged and neutral π and K mesons. Their property as messengers from the early reaction phase identifies them as potential probes for the high-density symmetry energy. Calculations show that the highest sensitivities may be expected at near-threshold energies.^{6,42,80} In both cases, collective flows or meson production, isotopic differences or ratios of observables are useful to minimize the sensitivity to the isoscalar part in the EoS while maximizing that to the symmetry term.

The FOPI Collaboration has collected an extensive set of π^-/π^+ production ratios measured for the four reactions $^{40}\text{Ca} + ^{40}\text{Ca}$, $^{96}\text{Zr} + ^{96}\text{Zr}$, $^{96}\text{Ru} + ^{96}\text{Ru}$, and $^{197}\text{Au} + ^{197}\text{Au}$ at several energies between 0.4 and 1.5 GeV/nucleon.⁴¹ Theoretical analyses of these data, however, have come to conflicting conclusions, suggesting everything from a rather stiff to a super-soft behavior of the symmetry energy.^{42–45} The reason may lie in the treatment of the pion in-medium and Δ dynamics^{78,81,82} and in competing effects of the mean fields and the Δ thresholds^{42,83} which will require further studies.⁸⁴ Cozma has demonstrated very recently that both types of observables, elliptic flow and pion production, can lead to compatible constraints for the stiffness of the symmetry energy, provided that care is taken to conserve the energy in inelastic collisions producing a Δ resonance.⁸¹ It may be done at a local or global level by accounting for the potential energy of hadrons in the treatment of two-body collisions. The sensitivity inherent in the spectral dependence of pion production has been pointed out by several authors.^{85–87} New information is expected to come from measurements performed by the S π RIT Collaboration^{87,88} at RIKEN with radioactive Sn beams.

4. Transport Theory

Common to all high-density probes is the need to relate the observations made for the asymptotic outcome of the reaction to the short interval during which the compressed matter exists and impacts the subsequent evolution. Heavy-ion collisions are non-equilibrium processes and non-equilibrium theory is, therefore, needed for their interpretation. Hydrodynamical or statistical descriptions may be useful for describing certain stages of the reaction process. A unified description requires transport theory to follow the evolution from the initial state of the collision system to the final stage when the strong interactions cease to act between its components. Such approaches have first been developed in the group of Walter Greiner

and at Michigan State University in the 80s,^{89–91} and have since evolved into a very valuable tool for extracting physics information from heavy-ion experiments.

Two families of transport approaches with different philosophies have been developed in nuclear physics. Those of the Boltzmann-Vlasov type (often named Boltzmann-Uehling-Uhlenbeck (BUU) approaches) describe the evolution in time of the one-body phase space density $f(\vec{r}, \vec{p}; t)$ under the influence of a mean field $U[f]$ and of two-body collisions

$$\begin{aligned} \frac{\partial f_1}{\partial t} + \frac{\vec{p}}{m} \nabla_{\vec{r}} f_1 - \nabla_{\vec{r}} U \nabla_{\vec{p}} f_1 = \\ \left(\frac{2\pi}{m}\right)^3 \int d\vec{p}_2 d\vec{p}_3 d\vec{p}_4 |\vec{v}_1 - \vec{v}_2| \sigma_{NN}(\Omega_{12}) \delta(\vec{p}_1 + \vec{p}_2 - \vec{p}_3 - \vec{p}_4) (f_3 f_4 \bar{f}_1 \bar{f}_2 - f_1 f_2 \bar{f}_3 \bar{f}_4). \end{aligned} \quad (4)$$

Here $f_i = f(\vec{r}, \vec{p}_i; t)$, $\bar{f}_i = (1 - f_i)$, v_i are velocities, and $\sigma_{NN}(\Omega)$ is the in-medium nucleon-nucleon (NN) cross-section. The potential $U[f]$ and the cross-section are either derived from an energy density functional, or are parametrized in order to test them relative to the data. If particle production, e.g. of pions and Δ resonances, is to be considered, additional physics input is needed: inelastic cross sections, potentials of the new particles, their cross sections for collisions with other particles and, possibly, the finite mass distributions of instable particles.

The solution of this equation is achieved with simulations using the test-particle (TP) method where the distribution function is represented in terms of finite elements as

$$f(\vec{r}, \vec{p}; t) = \frac{1}{N_{TP}} \sum_{i=1}^{AN_{TP}} g(\vec{r} - \vec{r}_i(t)) \tilde{g}(\vec{p} - \vec{p}_i(t)); \quad (5)$$

here N_{TP} is the number of TPs per nucleon, \vec{r}_i and \vec{p}_i are the time-dependent coordinates and momenta of the TPs, and g and \tilde{g} are the shape functions in coordinate and momentum space (e.g. δ -functions or Gaussians), respectively. Upon inserting this ansatz into the l.h.s. of Eq. 4, Hamiltonian equations of motion for the test particles are obtained, $\frac{d\vec{r}_i}{dt} = \frac{\vec{p}_i}{m}$ and $\frac{d\vec{p}_i}{dt} = -\vec{\nabla}_{\vec{r}_i} U$. The collision term is simulated stochastically, by performing TP collisions with a probability depending on the cross section and obeying the Pauli principle for the final state according to blocking factors $\bar{f}_i = (1 - f_i)$.

In the second family, the quantum molecular dynamics (QMD) model, the evolution of the collision is formulated in terms of the evolution of the coordinates $R_i(t)$ and momenta $P_i(t)$ of individual nucleons, similarly as in classical molecular dynamics, but with particles of finite width representing minimum nucleon wave packets. They move under the influence of NN forces. The method can also be viewed as being derived from the Time-Dependent Hartree (TDH) method with a product trial wave-function of single-particle states in Gaussian form. One obtains equations of motion of the same form as in BUU for the coordinates of the wave packets. Also a stochastic two-body collision term is introduced and treated in very

much the same way as in BUU, but now for nucleons and the full NN cross section. There are also relativistic formulations for both approaches using relativistic density functionals. Of the codes used in the analysis of the flow data discussed here UrQMD and TuQMD are relativistic codes, IQMD is non-relativistic. A review of the BUU method is given in Ref. 92 while the QMD method is reviewed in Ref. 93.

The main difference between the two approaches lies in the amount of fluctuations and correlations in the representation of the phase space distribution. In the BUU approach, the phase-space distribution function is seen as a smooth function of coordinates and momenta and can be increasingly better approximated by increasing the number of TPs. In the limit of $N_{\text{TP}} \rightarrow \infty$, the BUU equation is solved exactly but the solution is deterministic and contains neither fluctuations nor correlations. If they are considered to be important, as is the case when looking at cluster and fragment production, they have to be introduced explicitly through the Boltzmann-Langevin equation with a fluctuation term on the r.h.s. of Eq. 4. In the QMD, fluctuations are present because of the finite number of wave packets in the representation. In addition, classical correlations are present if explicit two-body interactions are used. The fluctuations in QMD-type codes are regulated and smoothed by choosing appropriate width parameters of the wave packets. QMD can be seen as an event generator solving the time evolution of different events independently. Event-by-event fluctuations are not even suppressed in the limit of infinitely many events.

The results of simulations with the two methods are thus expected to be similar, though not necessarily identical, as far as one-body observables are concerned as, e.g., the flow observables discussed in this article. Larger differences are expected for observables depending on fluctuations and correlations, such as the production of clusters and intermediate-mass fragments. Generally, the description of observables going beyond the mean field level is a question under active discussion in transport theory. In the experiment, copious numbers of light clusters and fragments are observed in heavy-ion collisions, particularly at lower energies.

In addition to these more fundamental differences between existing transport approaches, there are also differences that are caused by different implementations of the highly complex transport theories. Analyses of experimental data with seemingly similar physics input have lead to rather different conclusions. The analyses of the FOPI π^-/π^+ ratios represent an example. In order to reach a better understanding of possible reasons, a code-comparison project has been started. In a first publication, results for a standardized heavy-ion collision with identical physics input were compared.⁹⁴ Eighteen commonly used transport codes, nine of BUU and nine of QMD type, were included. Quantitatively, the differences were found to depend on the incident energy and amounted to approximately 30% at 100 and 15% at 400 MeV/nucleon, respectively. The comparison is presently continued with calculations for infinite nuclear matter. There the different ingredients of the transport codes can be tested separately and compared to exact limits.

5. Elliptic Flow

A "flow of nuclear matter out of the regions of compressed densities" was already predicted by Scheid, Ligensa and Greiner 49 years ago when they investigated central collisions of ^{16}O nuclei.⁹ The transverse emission of nuclear matter from the compressed interaction zone, the squeeze-out as it has been termed, has first been observed in experiments at the Bevalac.⁹⁵ In a sphericity analysis, the event shape in three dimensions was characterized by a kinetic-energy flow tensor whose main orientation with respect to the beam direction represents the collective sideways or directed flow. A difference in the two minor axes indicates the existence of elliptic flow. At the bombarding energies of up to several GeV/nucleon investigated in these studies, a preferential emission of charged particles perpendicular to the reaction plane has been observed. The shadowing by the spectator remnants reduces the in-plane flow, so that the strength of the off-plane emission, as quantified by the azimuthal anisotropy, reflects the internal pressure.

It has become customary to express both, directed and elliptic flows, and also possible higher flow components by means of a Fourier decomposition of the azimuthal distributions measured with respect to the orientation of the reaction plane ϕ_R ,^{96,97}

$$\frac{dN}{d(\phi - \phi_R)} = \frac{N_0}{2\pi} \left(1 + 2 \sum_{n \geq 1} v_n \cos n(\phi - \phi_R) \right), \quad (6)$$

where N_0 is the azimuthally integrated yield. The coefficients $v_n \equiv \langle \cos n(\phi - \phi_R) \rangle$ are functions of particle type, impact parameter, rapidity y , and the transverse momentum p_t ; v_1 and v_2 represent the directed and elliptic flows, respectively.

Elliptic flow has become an important observable at other energy regimes as well. At ultrarelativistic energies, the observation of the constituent-quark scaling of elliptic flow is one of the prime arguments for deconfinement during the early collision phase, and the behavior as an almost perfect liquid of the formed strongly interacting quark-gluon plasma are deduced from the observed magnitude of collective motions.^{98–101} It implies that elliptic flow develops very early in the collision which is valid also in the present range of relativistic energies, as confirmed by calculations.¹⁰² Isotopic flow differences appear thus very suitable for studying mean-field effects at high density.

An excitation function of the elliptic flow of $Z = 1$ particles in $^{197}\text{Au} + ^{197}\text{Au}$ collisions, compiled from various experiments,¹⁰³ is shown in Fig. 5. Squeeze-out perpendicular to the reaction plane, i.e. $v_2 < 0$, as a result of shadowing by the spectator remnants is observed at incident energies between about 150 MeV/nucleon and 4 GeV/nucleon with a maximum near 400 MeV/nucleon. At lower energies, the collective angular momentum in the mean-field dominated dynamics causes the observed in-plane enhancement of emitted reaction products. The figure also shows that elliptic flow can be measured quite precisely, as demonstrated by the good

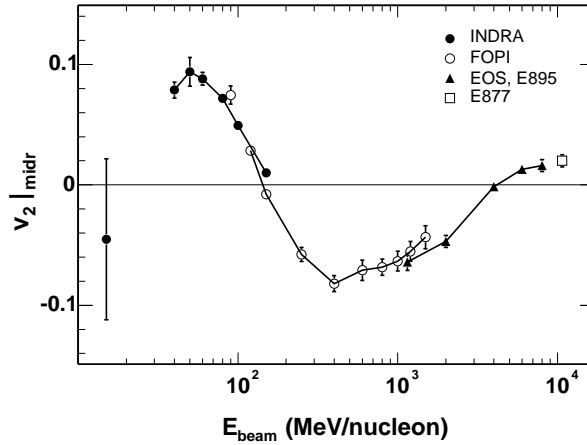


Fig. 5. Elliptic flow parameter v_2 at mid-rapidity for $^{197}\text{Au}+^{197}\text{Au}$ collisions at intermediate impact parameters ($\approx 5.5 - 7.5$ fm) as a function of incident energy. The filled and open circles represent the INDRA and FOPI data^{104,105} for $Z = 1$ particles, the triangles represent the EOS and E895 data¹⁰⁶ for protons, and the square represents the E877 data¹⁰⁷ for all charged particles (from Ref. 103, reprinted with kind permission from Springer Science+Business Media).

agreement of data sets from different experiments in the overlap regions of the studied intervals in collision energy.^{7,103,104}

The precision in interpreting the measured particle flows has been demonstrated by the FOPI Collaboration in their extensive report by Reisdorf *et al.*⁷ Calculations with the IQMD model were shown to account not only for the overall strength of the flow but also for the detailed dependence on rapidity and the change of sign of the v_2 parameter at rapidities $|y_0| \approx 0.7$; here y_0 is the rapidity normalized to the projectile rapidity in the c.m. system (Fig. 6). The approximately quadratic dependence of $v_2(y_0)$ has been fitted with two parameters, $v_2(y_0) = v_{20} + v_{22} \cdot y_0^2$, and a new quantity $v_{2n} = |v_{20}| + |v_{22}|$ has been introduced. It combines the information contained in the amplitude and the rapidity dependence of v_2 . The dependence of v_{2n} on the incident energy in the interval 0.4 to 1.5 GeV/nucleon covered by FOPI is fairly flat and its discriminating power between the soft and stiff parametrizations of the symmetric-matter EoS appears rather convincing.^{7,8}

6. Results from FOPI-LAND

The squeeze-out of neutrons has first been observed by the FOPI-LAND Collaboration who studied the reaction $^{197}\text{Au} + ^{197}\text{Au}$ at 400 MeV/nucleon.³⁸ The squeeze-out of charged particles reaches its maximum at this energy (Fig. 5), and similarly large anisotropies were observed for neutrons.³⁹ The neutrons had been detected with the Large-Area Neutron Detector, LAND,⁴⁹ while the FOPI Forward Wall, covering the forward hemisphere of laboratory angles $\theta_{\text{lab}} \leq 30^\circ$ with more than

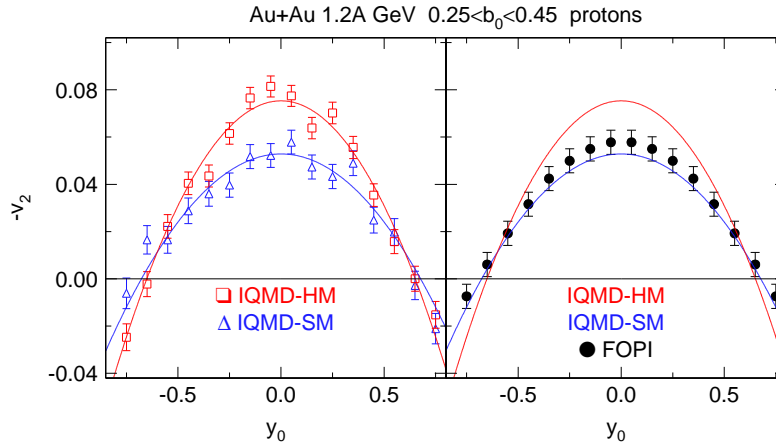


Fig. 6. Elliptic flow parameter $-v_2$ (note the change of sign) of protons as a function of the normalized rapidity y_0 for $^{197}\text{Au} + ^{197}\text{Au}$ collisions at 1.2 GeV/nucleon and the indicated near-central interval of normalized impact parameters b_0 . Left panel: IQMD calculations (symbols) for a hard (HM) and a soft (SM) EoS, both with momentum dependent forces, and the fit results (lines) assuming a quadratic dependence on y_0 . Right panel: The obtained fit results (lines) in comparison with the experimental data (symbols) measured with the FOPI detector at the GSI laboratory (reprinted from Ref. 8, Copyright (2016), with permission from Elsevier).

700 plastic scintillator elements, was used to determine the modulus and azimuthal orientation of the impact parameter.

The motivation for returning to the existing data set has been provided by studies performed with the UrQMD transport code for this fairly neutron-rich system ($N/Z = 1.49$). They indicated a significant sensitivity of the elliptic-flow parameters to the assumptions made for the density dependence of the symmetry energy.³⁷ In calculations with power-law coefficients $\gamma = 0.5$ and 1.5 (cf. Eq. 2 and Fig. 4), the relative strengths of neutron and proton elliptic flows were found to vary on the level of 15%.

The reanalysis of the data consisted mainly in choosing equal acceptances for neutrons and hydrogen isotopes with regard to particle energy, rapidity and transverse momentum (energy and momentum per nucleon for deuterons and tritons). The theoretical predictions have been obtained simulating the LAND acceptance and the experimental analysis conditions and were found to follow qualitatively the experimental data.

For the quantitative evaluation, the ratio of the flow parameters of neutrons versus protons or versus $Z = 1$ particles has been proposed as a useful observable.³⁷ Systematic effects influencing the collective flows of neutrons and charged particles in similar ways should thereby be minimized, on the experimental as well as on the theoretical side. In consideration of the systematic and experimental errors, a value $\gamma = 0.9 \pm 0.4$ has been adopted by the authors as best representing the power-law exponent of the potential term resulting from the elliptic-flow analysis.³⁷ It falls

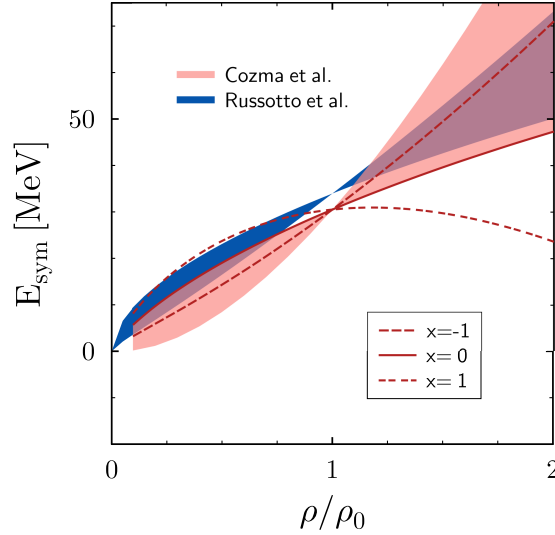


Fig. 7. Constraints on the density dependence of the symmetry energy obtained by Cozma *et al.* from comparing predictions of the Tübingen QMD for the neutron-proton elliptic-flow difference and ratio to FOPI-LAND experimental data (Ref. 108). The result of Russotto *et al.* (Ref. 37) is also shown, together with the Gogny-inspired parametrization of the symmetry energy for three values of the stiffness parameter: $x = -1$ (stiff), $x = 0$, and $x = 1$ (soft) (from Ref. 108).

slightly below the linear $\gamma = 1.0$ line shown in Fig. 4. The corresponding slope parameter is $L = 83 \pm 26$ MeV. Comparing with the many-body theories shown in Fig. 3, the elliptic-flow result is in good qualitative agreement with the range spanned by the DBHF and variational calculations based on realistic nuclear forces.

In an independent analysis, Cozma has used data from the same experiment and investigated the influence of several parameters on the difference and ratio of the elliptic flows of protons and neutrons using the Tübingen version of the QMD transport model.^{108,109} They included the parametrization of the isoscalar EoS, the choice of various forms of free or in-medium nucleon-nucleon cross sections, and model parameters as, e.g., the widths of the wave packets representing nucleons. The interaction developed by Das *et al.* with an explicit momentum dependence of the symmetry energy part was used.^{66,67} In Fig. 7, the obtained constraint on the density dependence of the symmetry energy is presented. It is overall in agreement with the result reported by Russotto *et al.*³⁷ but has a larger uncertainty because the effects of exploring the full intervals of the above-mentioned theoretical parameters were taken into account in the error determination. A stiffness closely corresponding to the $x = -1$ scenario is clearly favored while a super-soft solution with $x = 1$ is ruled out.

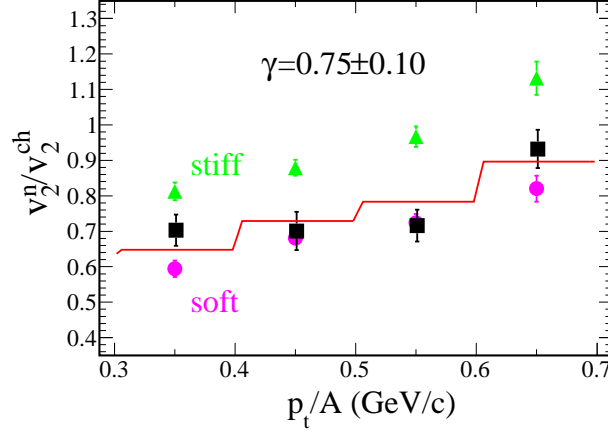


Fig. 8. Elliptic flow ratio of neutrons over all charged particles for central ($b < 7.5$ fm) collisions of $^{197}\text{Au}+^{197}\text{Au}$ at 400 MeV/nucleon as a function of the transverse momentum per nucleon p_t/A . The black squares represent the experimental data; the green triangles and purple circles represent the UrQMD predictions for stiff ($\gamma = 1.5$) and soft ($\gamma = 0.5$) power-law exponents of the potential term, respectively. The solid line is the result of a linear interpolation between the predictions, weighted according to the experimental errors of the included four bins in p_t/A and leading to the indicated $\gamma = 0.75 \pm 0.10$ (from Ref. 51).

7. Results from ASY-EOS

The experimental setup of the ASY-EOS experiment at the GSI laboratory followed the scheme developed for FOPI-LAND by using the Large Area Neutron Detector (LAND⁴⁹) as the main instrument for neutron and charged particle detection. For the event characterization and for measuring the orientation of the reaction plane, three detection systems had been installed. The ALADIN Time-of-Flight (AToF) Wall¹¹⁰ was used to detect charged particles and fragments in forward direction at polar angles up to $\theta_{\text{lab}} \leq 7^\circ$. Its capability of identifying large fragments and of characterizing events with a measurement of Z_{bound} ¹¹⁰ permitted the sorting of events according to impact parameter. Four double rings of the CHIMERA¹¹¹ multidetector carrying together 352 CsI(Tl) scintillators in forward direction and four rings with 50 thin CsI(Tl) elements of the Washington University Microball¹¹² array surrounding the target provided sufficient coverage and granularity for determining the orientation of the reaction plane from the measured azimuthal particle distributions. A detailed description of the experiment is available in Ref. 51.

The ratio v_2^n/v_2^{ch} obtained for the class of central ($b < 7.5$ fm) collisions as a function of the transverse momentum per nucleon p_t/A is shown in Fig. 8. The best description of the neutron-vs-charged-particle elliptic flow is obtained with a power-law coefficient $\gamma = 0.75 \pm 0.10$, where $\Delta\gamma = 0.10$ is the statistical uncertainty returned by the fit routine. It results from linearly interpolating between the predictions for the soft, $\gamma = 0.5$, and the stiff, $\gamma = 1.5$, predictions of the model within the range of transverse momentum $0.3 \leq p_t/A \leq 0.7$ GeV/c.

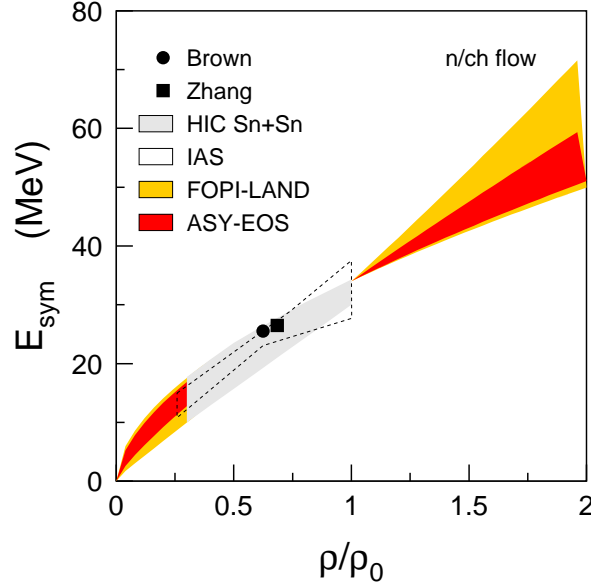


Fig. 9. Constraints deduced for the density dependence of the symmetry energy from the ASY-EOS data in comparison with the FOPI-LAND result of Ref. 37 as a function of the reduced density ρ/ρ_0 . The low-density results of Refs. 14, 34, 35 and 113 as reported in Ref. 16 are given by the symbols, the gray area (HIC), and the dashed contour (IAS). For clarity, the FOPI-LAND and ASY-EOS results are not displayed in the interval $0.3 < \rho/\rho_0 < 1.0$ (from Ref. 51).

With all corrections and errors included, the acceptance-integrated elliptic-flow ratio leads to a power-law coefficient $\gamma = 0.72 \pm 0.19$. This is the result displayed in Fig. 9 as a function of the reduced density ρ/ρ_0 . The new result confirms the former and has a considerably smaller uncertainty. It is also worth noting that the present parametrization is compatible with the low-density behavior of the symmetry energy from Refs. 14, 34, 35 and 113 that are included in the figure. The corresponding slope parameter describing the variation of the symmetry energy with density at saturation is $L = 72 \pm 13$ MeV.

The effective density probed with the elliptic flow measurement was explored in a study using again the Tübingen version¹⁰⁸ of the QMD model. The underlying idea consisted in performing transport calculations for the present reaction with two parametrizations of the symmetry energy that were chosen to be different for a selected range of density and identical elsewhere. The magnitude of the obtained difference between the two predictions for the elliptic flow ratio is considered a measure of the sensitivity to the selected density region.

It was found that the sensitivity achieved with the elliptic-flow ratio of neutrons over charged particles, the case chosen for the ASY-EOS analysis, reaches its maximum close to saturation density but extends beyond twice that value. Interestingly, the sensitivity of the neutron-vs-proton flow ratio has its maximum in the 1.4–1.5 ρ_0 region, i.e. at significantly higher densities than with light complex particles

being included. This observation contains an important potential for future experiments. With efficient isotope separation, flow measurements may give access to the curvature of the symmetry energy at saturation, in addition to the slope.

8. Conclusion and Outlook

The "flow of nuclear matter out of the regions of compressed densities" studied by Walter Greiner and his group⁹ many years ago has, in the meanwhile, evolved into a useful tool for the study of the nuclear equation of state (EoS) at high density. According to the predictions of transport models, the relative strengths of neutron and proton elliptic flows represent an observable sensitive to the symmetry energy at densities near and above saturation. By forming ratios or differences of neutron versus charged-particle flows, the influence of isoscalar-type parameters of the model descriptions can be minimized. As the interpretation of the FOPI pion ratios⁴¹ is not yet conclusive, this observable is presently unique as a terrestrial source of information for the EoS of asymmetric matter at high densities.

The value $\gamma = 0.72 \pm 0.19$ obtained in the ASY-EOS experiment for the power-law coefficient of the potential part in the UrQMD parametrization of the symmetry energy and the slope parameter $L = 72 \pm 13$ MeV are equivalent to a symmetry pressure $p_0 = \rho_0 L/3 = 3.8 \pm 0.7$ MeVfm⁻³. The latter may be used to estimate the pressure in neutron-star matter at saturation density. For an assumed asymmetry $\delta = (\rho_n - \rho_p)/\rho = 0.9$ in that part of the star, it amounts to 3.4 MeVfm⁻³ (Ref. 51), a value that compares well with the pressure obtained by Steiner *et al.*¹¹⁴ from neutron-star observations.

The study of the parameter dependence has shown that the contributions of the isoscalar sector are still significant. It will, therefore, be important to improve the description of the nuclear interaction in transport models, to reduce the parameter ranges also in the isoscalar sector, to improve the algorithms used for clusterization, as well as going beyond the mean-field picture, including short-range correlations.²⁹ Moreover, it will be quite important to compare the experimental data with the predictions of several transport models, of both Boltzmann-Vlasov and molecular-dynamics type, in order to pursue the work towards a model-independent constraint of the high-density symmetry energy initiated in Refs. 108 and 109.

The presented experimental results and the theoretical study of the density range that has been probed, provide a strong encouragement for continuing the flow measurements with improved detection systems. Model studies indicate that the sensitivity to the stiffness of the symmetry energy is still significant at incident energies as high as 800 MeV or 1 GeV/nucleon. The density study suggests that the range of densities that can be probed in the laboratory may reach up to twice or three times the saturation value if higher precision and isotopic resolution for light charged particles can be achieved. Future experiments will, therefore, benefit from the improved capabilities of the NeuLAND detector¹¹⁵ presently constructed as part of the R^3B setup for experiments at FAIR.

Acknowledgments

Stimulating and fruitful discussions with M. Di Toro, W. Reisdorf, Yongjia Wang, and with the authors of Ref. 109, M. D. Cozma, A. Le Fèvre, Y. Leifels, Qingfeng Li, J. Lukasik, and P. Russotto are gratefully acknowledged. HHW is partially supported by the Universe cluster of excellence of the DFG Germany.

References

1. M. Danos and W. Greiner, *Phys. Rev.* **134**, B284 (1964).
2. R. Ligensa, W. Greiner and M. Danos, *Phys. Rev. Lett.* **16**, 364 (1966).
3. W. Scheid, H. Müller and W. Greiner, *Phys. Rev. Lett.* **32**, 741 (1974).
4. P. Danielewicz, R. Lacey and W. G. Lynch, *Science* **298**, 1592 (2002).
5. C. Sturm *et al.*, *Phys. Rev. Lett.* **86**, 39 (2001).
6. C. Fuchs, A. Faessler, E. Zabrodin and Yu-Ming Zheng, *Phys. Rev. Lett.* **86**, 1974 (2001).
7. W. Reisdorf *et al.*, *Nucl. Phys. A* **876**, 1 (2012).
8. A. Le Fèvre, Y. Leifels, W. Reisdorf, J. Aichelin and Ch. Hartnack, *Nucl. Phys. A* **945**, 112 (2016).
9. W. Scheid, R. Ligensa and W. Greiner, *Phys. Rev. Lett.* **21**, 1479 (1968).
10. J. M. Lattimer and M. Prakash, *Phys. Rep.* **442**, 109 (2007).
11. Bao-An Li, Lie-Wen Chen and Che Ming Ko, *Phys. Rep.* **464**, 113 (2008).
12. M. Di Toro, V. Baran, M. Colonna and V. Greco, *J. Phys. G* **37**, 083101 (2010).
13. Topical Issue on Nuclear Symmetry Energy, *Eur. Phys. Jour. A* **50**, number 2 (2014).
14. M. B. Tsang, Yingxun Zhang, P. Danielewicz, M. Famiano, Z. Li, W. G. Lynch and A. W. Steiner, *Phys. Rev. Lett.* **102**, 122701 (2009).
15. M. B. Tsang *et al.*, *Phys. Rev. C* **86**, 015803 (2012).
16. C. J. Horowitz, E. F. Brown, Y. Kim, W. G. Lynch, R. Michaels, A. Ono, J. Piekarewicz, M. B. Tsang and H. H. Wolter, *J. Phys. G* **41**, 093001 (2014).
17. C. J. Horowitz and A. Schwenk, *Nucl. Phys. A* **776**, 55 (2006).
18. J. B. Natowitz *et al.*, *Phys. Rev. Lett.* **104**, 202501 (2010).
19. S. Typel, G. Röpke, T. Klähn, D. Blaschke and H. H. Wolter, *Phys. Rev. C* **81**, 015803 (2010).
20. L. Qin *et al.*, *Phys. Rev. Lett.* **108**, 172701 (2012).
21. B. A. Brown, *Phys. Rev. Lett.* **85**, 5296 (2000).
22. C. Fuchs and H. H. Wolter, *Eur. Phys. J. A* **30**, 5 (2006).
23. R. Subedi *et al.*, *Science* **320**, 1476 (2008).
24. O. Hen *et al.*, *Science* **346**, 614 (2014).
25. Chang Xu and Bao-An Li, *Phys. Rev. C* **81**, 064612 (2010).
26. A. W. Steiner and S. Gandolfi, *Phys. Rev. Lett.* **108**, 081102 (2012).
27. A. Carbone, A. Polls and A. Rios, *Europhys. Lett.* **97**, 22001 (2012).
28. Or Hen, Bao-An Li, Wen-Jun Guo, L. B. Weinstein and E. Piasetzky, *Phys. Rev. C* **91**, 025803 (2015).
29. Gao-Chan Yong, *Phys. Rev. C* **93**, 044610 (2016).
30. Bao-An Li and Xiao Han, *Phys. Lett. B* **727**, 276 (2013).
31. V. Baran, M. Colonna, V. Greco and M. Di Toro, *Phys. Rep.* **410**, 335 (2005).
32. A. Klimkiewicz *et al.*, *Phys. Rev. C* **76**, 051603(R) (2007).
33. A. Tamii *et al.*, *Phys. Rev. Lett.* **107**, 062502 (2011).
34. Zhen Zhang and Lie-Wen Chen, *Phys. Lett. B* **726**, 234 (2013).
35. B. A. Brown, *Phys. Rev. Lett.* **111**, 232502 (2013).

36. Bao-An Li, *Phys. Rev. Lett.* **88**, 192701 (2002).
37. P. Russotto *et al.*, *Phys. Lett. B* **697**, 471 (2011).
38. Y. Leifels *et al.*, *Phys. Rev. Lett.* **71**, 963 (1993).
39. D. Lambrecht *et al.*, *Z. Phys. A* **350**, 115 (1994).
40. W. Trautmann and H. H. Wolter, *Int. J. Mod. Phys. E* **21**, 1230003 (2012).
41. W. Reisdorf *et al.*, *Nucl. Phys. A* **781**, 459 (2007).
42. G. Ferini *et al.*, *Nucl. Phys. A* **762**, 147 (2005); *Phys. Rev. Lett.* **97**, 202301 (2006).
43. Zhigang Xiao *et al.*, *Phys. Rev. Lett.* **102**, 062502 (2009).
44. Zhao-Qing Feng and Gen-Ming Jin, *Phys. Lett. B* **683**, 140 (2010).
45. Wen-Jie Xie, Jun Su, Long Zhua and Feng-Shou Zhang *Phys. Lett. B* **718**, 1510 (2013).
46. Bao-An Li *et al.*, *J. Phys. Conf. Ser.* **312**, 042006 (2011).
47. De-Hua Wen, Bao-An Li and Lie-Wen Chen, *Phys. Rev. Lett.* **103**, 211102 (2009).
48. M. D. Cozma, *Phys. Lett. B* **700**, 139 (2011).
49. Th. Blaich *et al.*, *Nucl. Instrum. Methods Phys. Res. A* **314**, 136 (1992).
50. A. Pagano *et al.*, *Nucl. Phys. A* **734**, 504 (2004).
51. P. Russotto *et al.*, *Phys. Rev. C* **94**, 034608 (2016).
52. M. Baldo, C. Maieron, P. Schuck and X. Viñas, *Nucl. Phys. A* **736**, 241 (2004).
53. K. Fukukawa, M. Baldo, G. F. Burgio, L. Lo Monaco and H.-J. Schulze, *Phys. Rev. C* **92**, 065802 (2015).
54. C. Drischler, A. Carbone, K. Hebeler and A. Schwenk, *Phys. Rev. C* **94**, 054307 (2016).
55. R. B. Wiringa and S. C. Pieper, *Phys. Rev. Lett.* **89**, 182501 (2002).
56. F. Burgio, *J. Phys. G* **35**, 014048 (2008).
57. K. Hebeler, J. M. Lattimer, C. J. Pethick and A. Schwenk, *Phys. Rev. Lett.* **105**, 161102 (2010).
58. A. W. Steiner, J. M. Lattimer and E. F. Brown, *ApJ* **722**, 33 (2010).
59. see, e.g., the NASA website for the Neutron star Interior Composition ExploreR Mission (NICER), <https://heasarc.gsfc.nasa.gov/docs/nicer/>
60. V. Giordano, M. Colonna, M. Di Toro, V. Greco and J. Rizzo, *Phys. Rev. C* **81**, 044611 (2010).
61. Zhao-Qing Feng, *Phys. Lett. B* **707**, 83 (2012).
62. Xiao-Hua Li, Wen-Jun Guo, Bao-An Li, Lie-Wen Chen, F. J. Fattoyev and W. G. Newton, *Phys. Lett. B* **743**, 408 (2015).
63. D. D. S. Coupland *et al.*, *Phys. Rev. C* **94**, 011601(R) (2016).
64. Yingxun Zhang, M. B. Tsang, Zhuxia Li, Hang Liu, *Phys. Lett. B* **732**, 186 (2014).
65. Qingfeng Li, Zhuxia Li, S. Soff, M. Bleicher and H. Stöcker, *J. Phys. G* **32**, 151 (2006); *ibid.* **32**, 407 (2006).
66. C. B. Das, S. Das Gupta, C. Gale and Bao-An Li, *Phys. Rev. C* **67**, 034611 (2003).
67. Bao-An Li and Lie-Wen Chen, *Phys. Rev. C* **72**, 064611 (2005).
68. Yongjia Wang, Chenchen Guo, Qingfeng Li, Hongfei Zhang, Y. Leifels and W. Trautmann, *Phys. Rev. C* **89**, 044603 (2014).
69. Chenchen Guo, Yongjia Wang, Qingfeng Li, W. Trautmann, Ling Liu and LiJuan Wu, *Science China Physics, Mechanics & Astronomy* **55**, 252 (2012).
70. J. M. Lattimer and Y. Lim, *Astrophys. J.* **771**, 51 (2013).
71. B. G. Todd-Rutel and J. Piekarewicz, *Phys. Rev. Lett.* **95**, 122501 (2005).
72. X. Roca-Maza, M. Centelles, X. Viñas and M. Warda, *Phys. Rev. Lett.* **106**, 252501 (2011).
73. S. Typel and B. A. Brown, *Phys. Rev. C* **64**, 027302 (2001).
74. R. J. Furnstahl, *Nucl. Phys. A* **706**, 85 (2002).
75. C. J. Horowitz *et al.*, *Phys. Rev. C* **85**, 032501(R) (2012).
76. S. Abrahamyan *et al.*, *Phys. Rev. Lett.* **108**, 112502 (2012).

77. Bao-An Li, *Nucl. Phys. A* **708**, 365 (2002).
78. Jun Xu, Lie-Wen Chen, Che Ming Ko Bao-An Li and Yu Gang Ma, *Phys. Rev. C* **87**, 067601 (2013).
79. V. Greco, V. Baran, M. Colonna, M. Di Toro, T. Gaitanos and H. H. Wolter, *Phys. Lett. B* **562**, 215 (2003).
80. X. Lopez *et al.*, *Phys. Rev. C* **75**, 011901(R) (2007).
81. M. D. Cozma, *Phys. Lett. B* **753**, 166 (2016).
82. N. Ikeno, A. Ono, Y. Nara and A. Ohnishi, *Phys. Rev. C* **93**, 044612 (2016).
83. Taesoo Song and Che Ming Ko, *Phys. Rev. C* **91**, 014901 (2015).
84. Bao-An Li, *Phys. Rev. C* **92**, 034603 (2015).
85. Jun Hong and P. Danielewicz, *Phys. Rev. C* **90**, 024605 (2014).
86. M. D. Cozma, *Phys. Rev. C* **95**, 014601 (2017).
87. M. B. Tsang *et al.*, *Phys. Rev. C* **95**, 044614 (2017).
88. R. Shane *et al.*, *Nucl. Instrum. Methods Phys. Res. A* **784**, 513 (2015).
89. G. F. Bertsch, H. Kruse and S. Das Gupta, *Phys. Rev. C* **29**, 673 (1984).
90. H. Kruse, B. V. Jacak, J. J. Molitoris, G. D. Westfall and H. Stöcker, *Phys. Rev. C* **31**, 1770 (1985).
91. J. Aichelin and H. Stöcker, *Phys. Lett. B* **176**, 14 (1986).
92. G. F. Bertsch and S. Das Gupta, *Phys. Rep.* **160**, 189 (1988).
93. J. Aichelin, *Phys. Rep.* **202**, 233 (1991).
94. Jun Xu *et al.*, *Phys. Rev. C* **93**, 044609 (2016).
95. H. H. Gutbrod *et al.*, *Phys. Rev. C* **42**, 640 (1990).
96. J.-Y. Ollitrault, preprint arXiv:nucl-ex/9711003 (1997).
97. A. M. Poskanzer and S. A. Voloshin, *Phys. Rev. C* **58**, 1671 (1998).
98. B. I. Abelev *et al.*, *Phys. Rev. Lett.* **99**, 112301 (2007).
99. R. Fries, V. Greco and P. Sorensen, *Annu. Rev. Nucl. Part. Sci.* **58**, 177 (2008).
100. A. Adare *et al.*, *Phys. Rev. C* **85**, 064914 (2012).
101. U. W. Heinz and R. Snellings, *Annu. Rev. Nucl. Part. Sci.* **63**, 123 (2013).
102. P. Danielewicz, *Nucl. Phys. A* **673**, 375 (2000) 375.
103. A. Andronic, J. Lukasik, W. Reisdorf and W. Trautmann, *Eur. Phys. J. A* **30**, 31 (2006).
104. J. Lukasik *et al.*, *Phys. Lett. B* **608**, 223 (2005).
105. A. Andronic *et al.*, *Phys. Lett. B* **612**, 173 (2005).
106. C. Pinkenburg *et al.*, *Phys. Rev. Lett.* **83**, 1295 (1999).
107. P. Braun-Munzinger and J. Stachel, *Nucl. Phys. A* **638**, 3c (1998).
108. M. D. Cozma, Y. Leifels, W. Trautmann, Q. Li and P. Russotto, *Phys. Rev. C* **88**, 044912 (2013).
109. P. Russotto, M. D. Cozma, A. Le Fèvre, Y. Leifels, R. Lemmon, J. Lukasik, Q. Li and W. Trautmann, *Eur. Phys. J. A* **50**, 38 (2014).
110. A. Schüttauf *et al.*, *Nucl. Phys. A* **607**, 457 (1996).
111. A. Pagano *et al.*, *Nucl. Phys. A* **734**, 504 (2004).
112. D. G. Sarantites *et al.*, *Nucl. Instr. and Meth. A* **381**, 418 (1996).
113. P. Danielewicz and J. Lee, *Nucl. Phys. A* **922**, 1 (2014).
114. A. W. Steiner, J. M. Lattimer and E. F. Brown, *Astrophys. J. Lett.* **765**, L5 (2013).
115. NeuLAND Technical Design Report, submitted to FAIR (2011).